Receiver Structure and Performance for Trellis-Coded Pulse-Position Modulation in Optical Communication Systems

M. Srinivasan[1]

This article describes a receiver structure for trellis-coded pulse-position modulation (T-PPM) for optical communication systems. Monte Carlo simulation results of the Viterbi decoding algorithm under realistic Webb modeling of the avalanche photodiode (APD)-based receiver are compared with asymptotic bounds on performance. These results show that T-PPM can reduce the loss in performance incurred by spreading of the PPM optical pulse. Specifically, when a PPM symbol-error rate of 0.001 is required, the average signal photon count per information bit is reduced by 5 photons per information bit, or 0.6 to 2.0 dB depending upon the background photon level, when T-PPM is used with the receiver parameters selected here. It is also shown that preserving only a small subset of slot statistics during the decoding process does not result in any significant loss in overall performance.

I. Introduction

Current designs for deep-space optical communication systems utilize Q-switched lasers, which can provide peak power levels sufficient for deep-space applications. Because the duration of the optical pulse generated by the Q-switched laser is difficult to modify, the toggle rate between the on and off states is limited by the time it takes to recharge the lasing material. Given this constraint, pulse-position modulation (PPM) has been chosen over on–off keying as a more efficient signaling format. In M-ary PPM signaling, one of M symbols is transmitted in the form of a laser pulse located in one of M time slots in order to transmit $\log_2 M$ bits of data.

In the receivers considered in this article, an avalanche photodiode (APD) is used to detect the downlink optical signal. The APD generates a random number of electrons in response to each photon absorbed from the received signal. The number of electrons that the APD outputs over a specified time interval is governed by the McIntyre–Conradi distribution, which is closely approximated by the Webb distribution. In addition, Gaussian thermal noise induced by receiver electronics contributes to the current response of the detector. The APD output is integrated over each slot duration, resulting in M slot statistics per PPM symbol. The density of these slot statistics is modeled as a mixture density consisting of the convolution of Webb and Gaussian density functions. Assuming that the slot statistics are independent random

[1] Communications Systems and Research Section.

variables, the optimum PPM symbol demodulation strategy is to select the PPM symbol corresponding to the maximum slot statistic [1].

Because of the limitations on the Q-switched laser, the optical pulse shape may not be restricted to one slot interval and may spread over several slots. This results in a reduction of signal energy in the transmitted PPM symbol slot and a larger probability of another nearby slot statistic surpassing the transmitted slot statistic in value, thereby causing higher symbol-error probability. This effect also may occur on the receiving end in the form of pulse smearing as a result of limited detector bandwidth caused by large detector area. In order to combat these problems, trellis-coded modulation of the PPM symbols has been proposed. By partitioning the PPM symbol set into subsets of larger minimum distance, and by using convolutional encoding to select the signal subset from which to transmit the next PPM symbol, the symbol-error probability can be reduced substantially. In this article, the trellis-coded PPM (T-PPM) scheme proposed in [2] is reviewed, the decoding algorithm for T-PPM is described, and simulation results are presented for a rate 7/8 T-PPM system with Viterbi decoding using realistic modeling of the APD-based optical receiver.

II. System Model

Following the treatment in [2], the optical system under consideration is described as follows. The intensity of the received optical signal may be written as

$$\lambda_r(t) = \lambda_b + \lambda_s \sum_{i=-\infty}^{\infty} h(t - d_i T_{\text{slot}} - NiT_{sym}) \tag{1}$$

Here, λ_s denotes the peak intensity of the received optical signal and λ_b denotes the intensity of the background noise, both in absorbed photons per second. The optical pulse shape is $h(t)$, the PPM slot duration is T_{slot}, the PPM symbol duration is T_{sym}, and the ith PPM symbol value is d_i. Note that $d_i \in \{0, 1, \cdots, M-1\}$ and that $T_{sym} = MT_{\text{slot}}$. The parameter $N \geq 1$ is included to allow for a certain number of dead-time slots between PPM pulses. The value of N may be adjusted according to the amount of time required for the laser to recharge between generation of pulses.

The current response of the APD to the received photons is integrated over each slot interval of each transmitted symbol, resulting in NM slot statistics per PPM symbol duration, including dead-time slots. The lth slot statistic of the mth PPM symbol may be written as

$$X_{l,m} = qW(l,m) + \nu(l,m) \tag{2}$$

where q is the charge of an electron and $W(l,m)$ is the number of APD output electrons in the interval. The additional charge due to Gaussian thermal noise is $\nu(l,m)$ and has mean $I_s T_{\text{slot}}$ and variance $(qI_s + 2\kappa T/R)T_{\text{slot}}$, where I_s is the APD surface leakage current, κ is Boltzmann's constant, T is the equivalent noise temperature, and R is the load resistance. Note that the APD surface leakage current is not multiplied by the APD gain and is modeled here as a constant DC current. The APD dark current, however, is multiplied by the APD gain and may be incorporated into the value of λ_b as part of the background radiation. The random variable $W(l,m)$ depends upon the mean number of absorbed photons within the slot interval and is distributed according to the McIntyre distribution [3], which may be approximated using the Webb density function when the absorbed photons are Poisson distributed [4]. The Webb probability mass function for the distribution of APD output electrons depends upon the average number of photons absorbed and is given by

$$P[W(l,m) = n_2 | \bar{n}(l,m) = n_1] =$$

$$\frac{1}{\sqrt{2\pi n_1 G^2 F}\left(1 + \dfrac{n_2 - G n_1}{n_1 GF/(F-1)}\right)^{3/2}} \exp\left(-\frac{(n_2 - G n_1)^2}{2 n_1 G^2 F\left(1 + \dfrac{n_2 - G n_1}{n_1 GF/(F-1)}\right)}\right) \tag{3}$$

Here, $F = kG + (2 - 1/G)(1 - k)$, G is the APD gain, k is the APD ionization ratio, and $\bar{n}(l,m)$ is the mean number of photons absorbed over the lth time slot of the mth PPM symbol and is given by

$$\begin{aligned}
\bar{n}(l,m) &= \int_{(l+NMm)T_{\text{slot}}}^{(l+1+NMm)T_{\text{slot}}} \lambda_r(t)dt \\
&= \int_{(l+NMm)T_{\text{slot}}}^{(l+1+NMm)T_{\text{slot}}} \lambda_b dt + \int_{(l+NMm)T_{\text{slot}}}^{(l+1+NMm)T_{\text{slot}}} \lambda_s \sum_{i=-\infty}^{\infty} h(t - d_i T_{slot} - NiT_{sym})dt \\
&= \bar{n}_b + \bar{n}_s Y_{l,m}
\end{aligned} \tag{4}$$

where $\bar{n}_b = \lambda_b T_{\text{slot}}$, $\bar{n}_s = \lambda_s T_{\text{slot}}$, and

$$Y_{l,m} = \frac{1}{T_{\text{slot}}} \int_{(l+NMm)T_{\text{slot}}}^{(l+1+NMm)T_{\text{slot}}} \sum_{i=-\infty}^{\infty} h(t - d_i T_{\text{slot}} - NiT_{sym})dt \tag{5}$$

Note that $\bar{n}_s$ is intended to represent the average number of signal photons observed over an entire symbol interval, so that the signal energy of the transmitted laser pulse over one symbol duration remains constant as the pulse spreads out over more than one slot. On the other hand, $\bar{n}_s Y_{l,m}$, which is the average number of signal photons observed over the lth slot, decreases as the pulse spreads out in time. Ideally, the pulse shape $h(t)$ is a rectangular pulse of unit amplitude restricted to one slot in duration. This ideal shape results in the following values for $Y_{l,m}$ given the PPM symbol value $d_m = j$:

$$Y_{l,m}|_{d_m = j} = \begin{cases} 1 & l = j \\ 0 & l \neq j \end{cases} \tag{6}$$

However, if $h(t)$ contains the same energy but is spread out over several slots adjacent to slot j, $Y_{j,m}$ will be less than one, and $Y_{l,m}$ will be nonzero for several values of $l \neq j$. When noise is factored in, this situation leads to a greater number of incorrect decisions in picking the maximum slot statistic, resulting in a higher PPM symbol-error probability.

III. Trellis-Coded PPM: Encoding and Decoding

In order to combat the performance degradation caused by nonideal pulse shapes, the method of trellis-coded modulation was proposed in [2] for use with PPM signaling. The PPM symbol set is partitioned into subsets that consist of signals with a certain minimum distance, where distance is defined as the

number of time slots between PPM symbol positions. In the 256-ary PPM system considered here ($M = 256$), the set $A = \{0, 1, \cdots, 255\}$, which has minimum distance 1, is partitioned into the two subsets $B_0 = \{0, 2, \cdots, 254\}$ and $B_1 = \{1, 3, \cdots, 255\}$, which have minimum distance 2. Both B_0 and B_1 are divided again into $C_0 = \{0, 4, \cdots, 252\}$ and $C_2 = \{2, 6, \cdots, 254\}$, and $C_1 = \{1, 5, \cdots, 253\}$ and $C_3 = \{3, 7, \cdots, 255\}$, respectively, all of which have minimum distance 4. Although results are given here only for the four-partition case, the subsets C_i may be further partitioned if necessary. The set partitioning tree is shown in Fig. 1.

Once the set partitions have been established, convolutional encoding imparts a trellis structure upon the allowed PPM symbol sequence, resulting in greater minimum free distance. In our system, a rate 1/2 convolutional code is used to select one of the four signal partitions, while 6 other bits choose from among the signals within each partition, yielding a rate 7/8 trellis code. The encoder and resulting trellis of minimum distance 4 are shown in Figs. 2 and 3, respectively. The low-order input bit a_0 enters the convolutional encoder shown in Fig. 2, and the output bits b_0 and b_1 are used to choose paths to a particular signal subset as specified by the branch labels in Fig. 1. The remaining input bits a_1 through a_6 pass straight through as uncoded output bits b_2 through b_7 and determine which of the 64 signals within each subset is transmitted. Note that each trellis branch in Fig. 3 is actually a parallel transition labeled by the signal partition from which one of 64 signals may be selected for transmission. Once an 8-bit word has been selected for each trellis branch, the corresponding PPM symbol is transmitted.

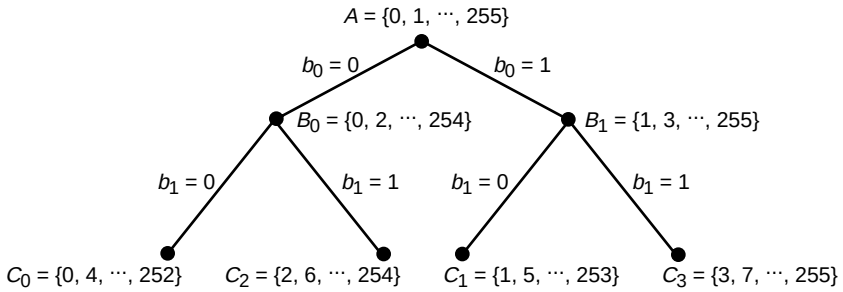

Fig. 1. Set partitions for 256-ary PPM signaling.

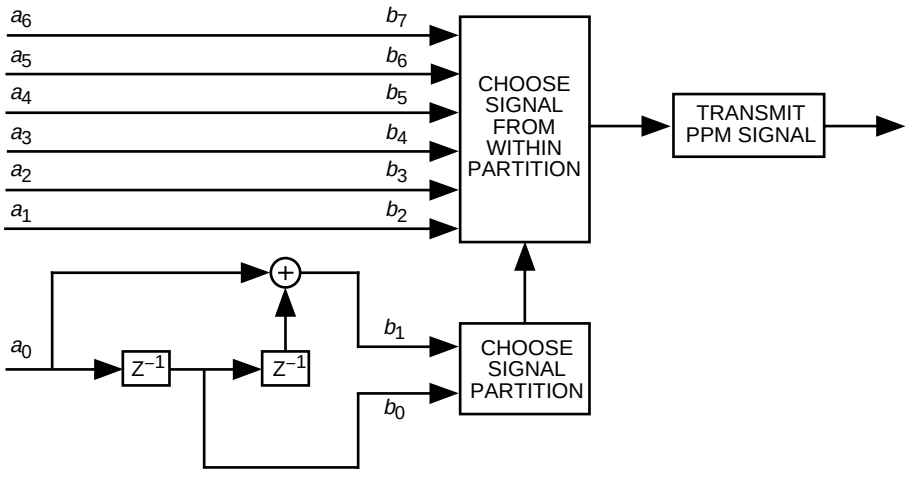

Fig. 2. The rate 7/8 trellis-coded PPM encoder.

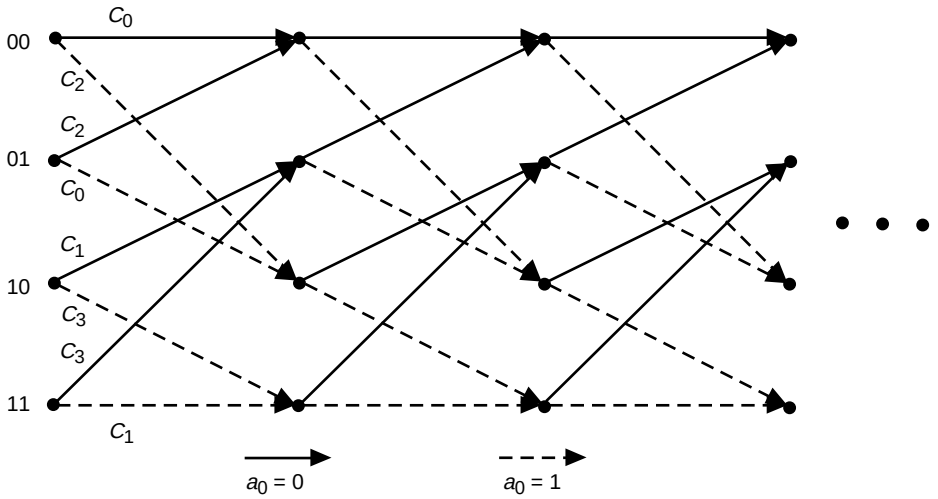

Fig. 3. The four-state trellis for rate 7/8 trellis-coded PPM.

The trellis structure of the transmitted sequence and low constraint length of the convolutional code suggest decoding through use of the Viterbi algorithm (as opposed to sequential decoding [5]). The decoding consists of the following steps (Fig. 4):

(1) For each PPM symbol time interval, 256 slot statistics are compiled (assuming PPM symbol boundaries are known and dead-time slots may be discounted).

(2) For each branch in the trellis, the 64 slot statistics corresponding to the 64 allowed signals for that branch are compared and the maximum slot statistic value is chosen. The identity of the PPM symbol corresponding to that maximum slot statistic is stored, and the value of the maximum slot statistic is saved as the metric for that branch. For any path through the trellis, the individual branch metrics along the path are added to form the accumulated metric for that path.

(3) The Viterbi algorithm is applied to the trellis. For each of the four state nodes in the trellis, the two incoming accumulated path metrics are compared and the path corresponding to the largest metric value is kept as the survivor while the other incoming path is discarded.

(4) A decision is made on the ith transmitted PPM symbol by looking at the partial path with the largest accumulated path metric at the $(i + D)$th stage in the trellis, where D is the user-specified decoding delay. The path with the largest accumulated metric at stage $i + D$ is traced back to stage i to retrieve the PPM symbol that was stored for that particular branch. This symbol is output as the decoded PPM symbol.

In our simulations, the decoding delay D is set to 10, which is 5 times the constraint length of the convolutional code used. Note that the branch metric used in the Viterbi algorithm is the maximum slot statistic value and is a heuristic metric chosen for its simplicity. The maximum-likelihood branch metric is based upon the likelihood function for the observables and is not included in this study.

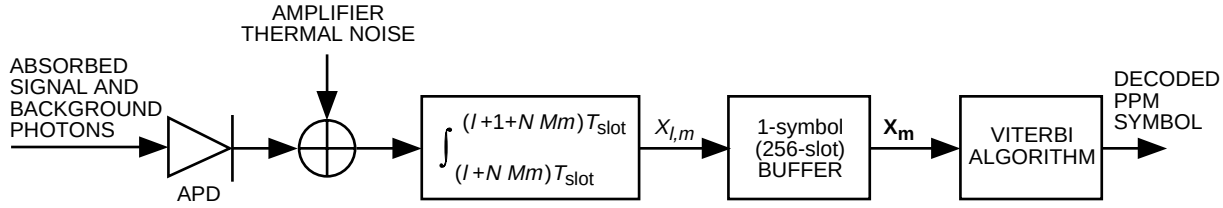

Fig. 4. The receiver structure for T-PPM.

IV. Performance Results

In [2], analytical results were given for the performance of uncoded PPM and trellis-coded PPM in the presence of imperfect pulse shaping. These results were based upon using the Gaussian approximation for APD output statistics and using the union bound to approximate PPM symbol-error probability. If the laser pulse obeys a Gaussian shape, i.e.,

$$h(t) = \frac{T_{\text{slot}}}{\sqrt{2\pi\sigma_h^2}} \exp\left(-\frac{\left(t - \frac{T_{\text{slot}}}{2}\right)^2}{2\sigma_h^2} \right) \tag{7}$$

where the standard deviation σ_h indicates the extent to which the laser pulse is smeared out in time, and if the Gaussian approximation is used for the distribution of the APD output, then the uncoded 256-ary PPM symbol-error probability may be approximated by [2]

$$P_{e,PPM} \approx \frac{1}{256} \sum_{j=0}^{255} \sum_{l \neq j} \frac{1}{2} \operatorname{erfc}\left(\frac{qG\bar{n}_s(Z_{j,j} - Z_{l,j})}{\sqrt{2\left(q^2G^2F[2\bar{n}_b + \bar{n}_s(Z_{j,j} + Z_{l,j})] + 2\left(\frac{2\kappa T}{R} + qI_s\right)T_{\text{slot}}\right)}} \right) \tag{8}$$

Here, $Z_{l,j} = Y_{l,n}|_{d_n=j}$, so that

$$Z_{j,j} - Z_{l,j} = 1 - \operatorname{erfc}\left(\frac{T_{\text{slot}}}{2\sqrt{2}\sigma_h}\right) - \frac{1}{2}\operatorname{erfc}\left(-\frac{T_{\text{slot}}\left(l - j + \frac{1}{2}\right)}{\sqrt{2}\sigma_h} \right) + \frac{1}{2}\operatorname{erfc}\left(-\frac{T_{\text{slot}}\left(l - j - \frac{1}{2}\right)}{\sqrt{2}\sigma_h} \right) \tag{9}$$

and

$$Z_{j,j} + Z_{l,j} = 1 - \operatorname{erfc}\left(\frac{T_{\text{slot}}}{2\sqrt{2}\sigma_h}\right) + \frac{1}{2}\operatorname{erfc}\left(-\frac{T_{\text{slot}}\left(l - j + \frac{1}{2}\right)}{\sqrt{2}\sigma_h} \right) - \frac{1}{2}\operatorname{erfc}\left(-\frac{T_{\text{slot}}\left(l - j - \frac{1}{2}\right)}{\sqrt{2}\sigma_h} \right) \tag{10}$$

Note that Eq. (8) assumes perfect symbol synchronization so that the dead-time slots may be located and ignored in making symbol decisions.

Calculation of the symbol-error probability for Viterbi decoding of trellis-coded PPM generally is quite difficult. In [2], an approximation is used to estimate the performance of T-PPM. As the number of signal photons per pulse becomes large in comparison with the background photon level and thermal noise, the symbol-error probability is dominated by the probability that the erroneous symbol sequences closest in distance to the transmitted PPM symbol sequence are selected by the decoder. For the four-state trellis used in the code described here, the minimum distance between any given symbol sequence and any other sequence that diverges from and remerges with the transmitted sequence is 4 and results from the selection of a symbol from the same subset, C_i, over one parallel branch transition. The probability of choosing the wrong symbol from within one parallel transition can be upper bounded using the union bound, resulting in the following approximation:

$$P_{e,T-PPM} \approx P\left[\bigcup_{j\in C_i, j\neq l} \text{decoder chooses symbol } j \text{ from set } C_i | \text{ symbol } l \in C_i \text{ sent}\right]$$

$$\leq 63 \times P\,[\text{ decoder chooses symbol at distance 4 from transmitted symbol}]$$

$$= \frac{63}{2}\,\text{erfc}\left(\frac{qG\bar{n}_s(Z_{l,l} - Z_{l+4,l})}{\sqrt{2\left(q^2G^2F[2\bar{n}_b + \bar{n}_s(Z_{l,l} + Z_{l+4,l})] + 2\left(\frac{2\kappa T}{R} + qI_s\right)T_{\text{slot}}\right)}}\right) \tag{11}$$

The values of $Z_{l,l} - Z_{l+4,l}$ and $Z_{l,l} + Z_{l+4,l}$ are found using Eqs. (9) and (10). Note that Approximation (11) is an asymptotic upper bound for the symbol-error probability.

In order to more reliably predict the photon levels required for a certain level of error-rate performance, Monte Carlo simulations were performed in which the more accurate Webb-plus-Gaussian mixture process was used to model the output of the APD in the presence of additive thermal noise. The Webb deviates needed to simulate the APD output were generated using the inclusion–exclusion method [6] following the technique outlined in [7]. The simulations were run using the following parameters: $T_{\text{slot}} = 2\times10^{-8}$ s, $G = 40.0$, $k = 0.007$, $I_s = 2 \times 10^{-9}$ A, $T = 300$ K, and $R = 146,650\ \Omega$. The simulations were performed for both uncoded 256-ary PPM as well as rate 7/8 trellis-coded PPM in order to measure the gain obtained by using trellis coding. The decoding delay for the Viterbi algorithm used in decoding the T-PPM signals was set to 10, which is adequate for a convolutional code of memory 2.

Two sets of simulation results are presented here. The first set represents results obtained when all slot statistics were available for processing as described in the decoding algorithm set forth in Section III. The second set of results was obtained from a system in which only the five slots with the largest APD output electron counts were preserved for use in decoding, while all other slot values were set to zero. In other words, step 1 of the decoding algorithm is modified so that there are only five nonzero slot statistics available for the subsequent decoding steps. This second set of simulations is intended to indicate the performance of a system with reduced memory capacity that may be utilized in a real receiver implementation. All of the simulations were performed using Gaussian shaped pulses that have standard deviation values $\sigma_h = 0.2T_{\text{slot}}$, $0.4T_{\text{slot}}$, and $0.6T_{\text{slot}}$. With $T_{\text{slot}} = 20$ ns, $\sigma_h = 0.2T_{\text{slot}}$ corresponds to a pulse more or less restricted to the 20-ns slot duration (98 percent of pulse energy within one slot). On the other hand, $\sigma_h = 0.4T_{\text{slot}}$ and $\sigma_h = 0.6T_{\text{slot}}$ correspond to pulses occupying 60 ns (three slot widths) and 80 ns (four slot widths), respectively. Note that, although the Gaussian pulse described in Eq. (7) extends across an infinite number of time slots, in the simulations, the Gaussian pulse is truncated to a finite number of slots.

Figures 5 through 10 contain results for the system in which all slot statistics are used. The plots in Figs. 5 and 6 show the mean absorbed signal photon level per symbol that is required for symbol-error probabilities of 0.01 and 0.001, respectively, as a function of mean absorbed background photon level per slot. Each plot shows the performance of uncoded PPM and T-PPM for the three different values of σ_h. From the uncoded PPM curves in these two figures, it may be seen that substantial degradation results from having pulses spread out over three or four slots ($\sigma_h = 0.4T_{\text{slot}}$ and $\sigma_h = 0.6T_{\text{slot}}$), as compared with the pulse restricted to one slot ($\sigma_h = 0.2T_{\text{slot}}$). The more extreme case of $\sigma_h = 0.6T_{\text{slot}}$ results in roughly a doubling of the required number of photons per pulse over the $\sigma_h = 0.2T_{\text{slot}}$ case. Trellis-coded PPM reduces the number of required photons per pulse by varying amounts, most significantly when $\sigma_h = 0.6T_{\text{slot}}$.

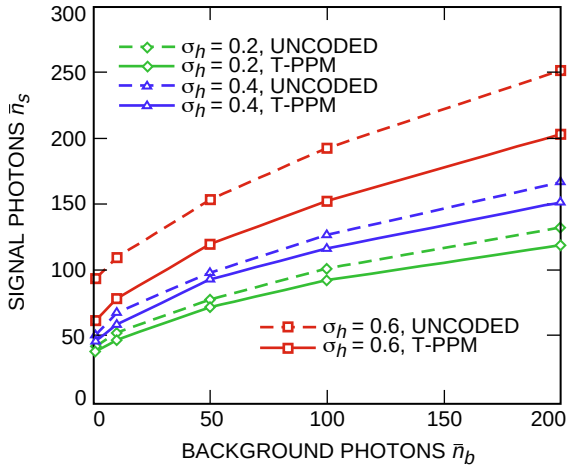

Fig. 5. Mean absorbed signal photons per pulse required for a symbol-error rate of 0.01.

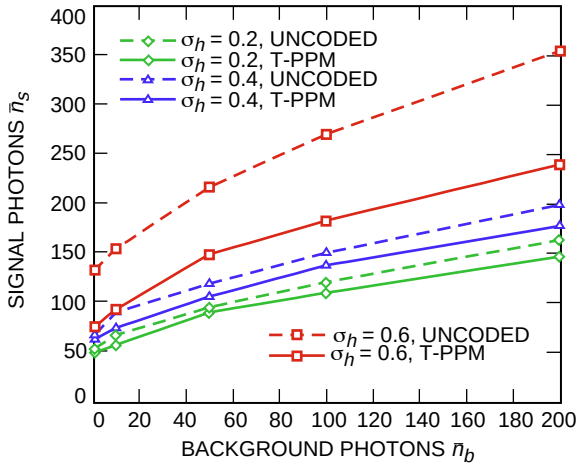

Fig. 6. Mean absorbed signal photons per pulse required for a symbol-error rate of 0.001.

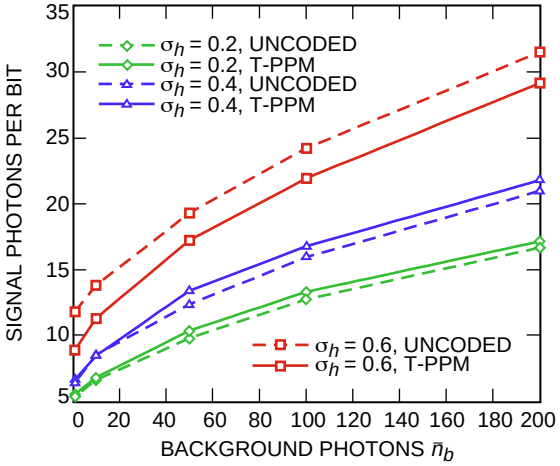

Fig. 7. Mean absorbed signal photons per information bit required for a symbol-error rate of 0.01.

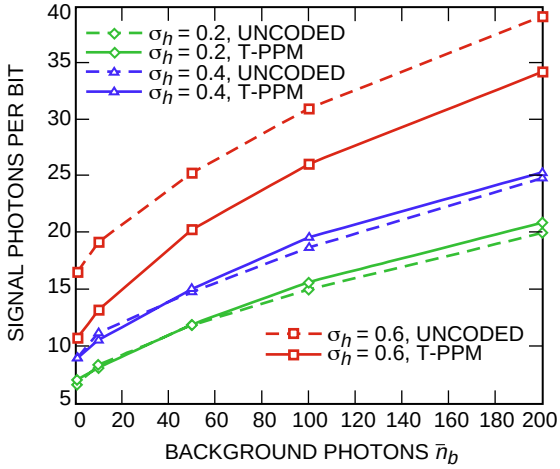

Fig. 8. Mean absorbed signal photons per information bit required for a symbol-error rate of 0.001.

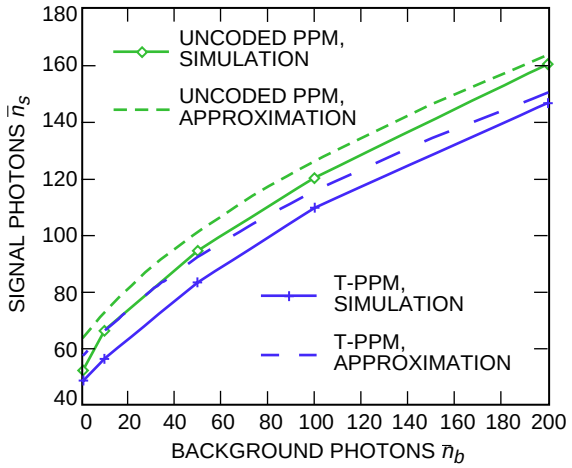

Fig. 9. Comparison of simulation results and analytical approximations for $\sigma_h = 0.2T_{slot}$, 0.001 symbol-error probability.

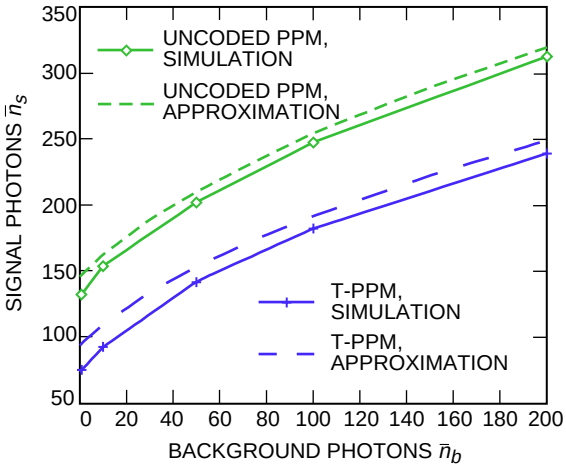

Fig. 10. Comparison of simulation results and analytical approximations for $\sigma_h = 0.6T_{slot}$, 0.001 symbol-error probability.

In order to account for the reduced information throughput of the rate 7/8 T-PPM signal as compared with uncoded PPM, the numbers in Figs. 5 and 6 are normalized so that the required number of signal photons per information bit can be considered. The results are shown in Figs. 7 and 8 for symbol-error probabilities of 0.01 and 0.001, respectively. These figures show that, when normalized for information bit rate, the T-PPM results show improved performance only when the pulse spreading is substantial, i.e., for $\sigma_h > 0.4T_{\text{slot}}$. This improvement is larger when the desired symbol-error probability is 0.001 (4- to 6-photon-per-bit gain) than when the desired symbol-error probability is 0.01 (2- to 3-photon-per-bit gain).

Figures 9 and 10 provide a comparison between the simulation results and results obtained from using the analytical expressions for symbol-error probabilities in [2] [given in Eqs. (8) and (11)] for the particular cases of $\sigma_h = 0.2T_{\text{slot}}$ and $\sigma_h = 0.6T_{\text{slot}}$ with a 0.001 PPM symbol-error probability. Note that the analytical curves upper bound the simulation results, but appear to be offset from the simulated curves by a fixed amount over a wide range of $\bar{n}_b$ values, and can be used to predict the improvement from uncoded PPM to T-PPM, if not the exact photon count values.

Figures 11 through 14 show results from the second set of simulations mentioned earlier, i.e., simulations of the T-PPM decoding obtained when using only the top 5 slot statistics per PPM symbol, with all remaining 251 statistics set to zero. The T-PPM results from the first set of simulations in which all slot statistics are used also are shown for comparison. Figures 11 and 12 show the mean absorbed signal photon level per symbol that is required for symbol-error probabilities of 0.01 and 0.001, respectively, as a function of mean absorbed background photon level per slot. Figures 13 and 14 show the required signal photon levels per information bit. Although there may be some slight variations between these curves and the curves obtained from using all slot statistics, the two sets of results are extremely close in value, and demonstrate that keeping only the top 5 slot statistics out of every PPM symbol does not deteriorate the performance of T-PPM significantly.

V. Conclusions

In this article, the receiver structure and simulation results for demodulation of the trellis-coded PPM signaling scheme described in [2] were presented. The performance gain of T-PPM over uncoded PPM in the presence of optical pulse spreading that was described in [2] (based upon Gaussian channel modeling) was verified here by using more realistic channel models and Monte Carlo simulations of receiver performance. It was shown that a 5-photon-per-information-bit improvement in required signal strength can be achieved by using T-PPM when the laser pulse spreads over 4 slot widths and the required PPM symbol-error probability is 0.001, which corresponds to a 2-dB gain at low background photon levels. The performance gain decreases somewhat when the required symbol-error probability is 0.01, and also decreases when the laser pulse is spread out over less than 4 slots. In addition, simulations were performed for a modified receiver structure in which only the 5 slots with the largest APD output electron counts were preserved from each PPM symbol, while all other slot statistics in each PPM symbol were set to zero. This modified structure showed almost no deterioration in T-PPM performance relative to the receiver that used all slot statistics in the Viterbi decoding algorithm.

Further improvements upon the T-PPM receiver structure may lie in optimizing the branch metric used in Viterbi decoding. In this article, the maximum slot statistic value over all signals contained within the partition associated with a particular transition was used as the branch metric and is suboptimal. The maximum-likelihood branch metric is based upon the likelihood function for the slot statistics and will depend upon how the channel is modeled. The Webb–Gaussian mixture density used in the simulations presented here may lead to a fairly complicated likelihood function that is computationally prohibitive to implement but may nonetheless lead to improved performance.

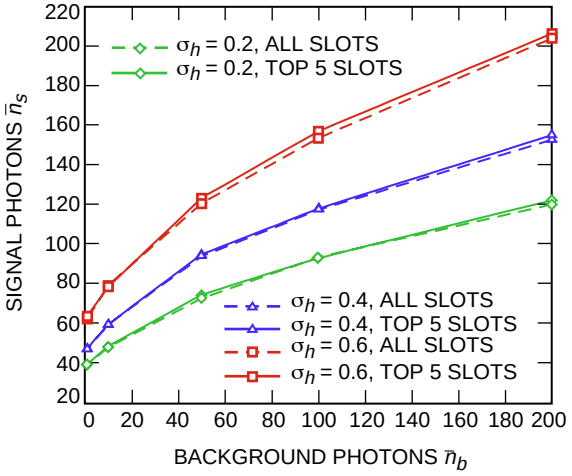

Fig. 11. Mean absorbed signal photons per pulse required for T-PPM with a symbol-error rate of 0.01: top five slot statistics versus all slot statistics used in decoding.

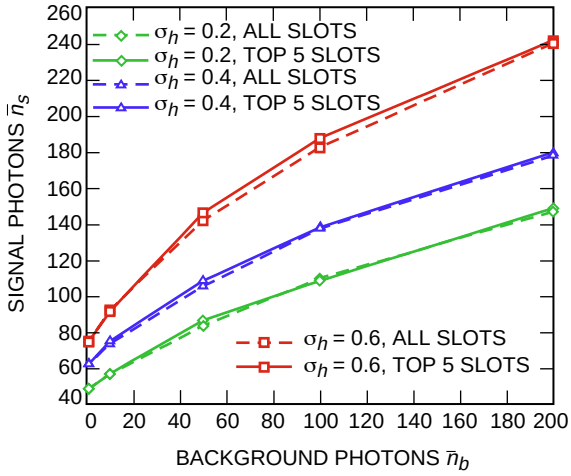

Fig. 12. Mean absorbed signal photons per pulse required for T-PPM with a symbol-error rate of 0.001: top five slot statistics versus all slot statistics used in decoding.

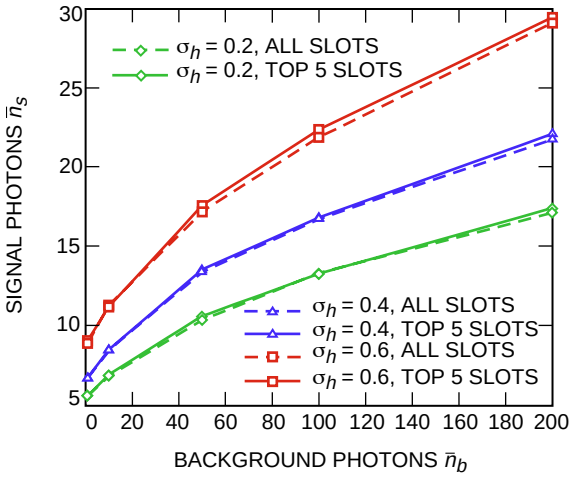

Fig. 13. Mean absorbed signal photons per information bit required for T-PPM with a symbol-error rate of 0.01: top five slot statistics versus all slot statistics used in decoding.

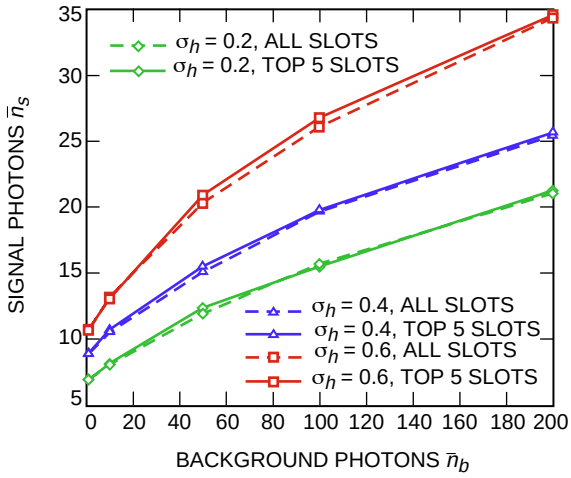

Fig. 14. Mean absorbed signal photons per information bit required for T-PPM with a symbol-error rate of 0.001: top five slot statistics versus all slot statistics used in decoding.

References

[1] V. Vilnrotter, M. Simon, and M. Srinivasan, *Maximum Likelihood Detection of PPM Signals Governed by an Arbitrary Point Process Plus Additive Gaussian Noise*, JPL Publication 98-7, Jet Propulsion Laboratory, Pasadena, California, April 1998.

[2] K. Kiasaleh and T.-Y. Yan, "T-PPM: A Novel Modulation Scheme for Optical Communication Systems Impaired by Pulse-Width Inaccuracies," *The Telecommunications and Mission Operations Progress Report 42-135, July–September 1998*, Jet Propulsion Laboratory, Pasadena, California, pp. 1–16, November 15, 1998.
http://tmo.jpl.nasa.gov/tmo/progress_report/42-135/135G.pdf

[3] R. J. McIntyre, "The Distribution of Gains in Uniformly Multiplying Avalanche Photodiodes: Theory," *IEEE Transactions on Electron. Devices*, vol. ED-19, no. 6, pp. 703–713, June 1972.

[4] P. P. Webb, R. J. McIntyre, and J. Conradi, "Properties of Avalanche Photodiodes," *RCA Review*, vol. 35, pp. 234–278, June 1974.

[5] S. B. Wicker, *Error Control Systems for Digital Communication and Storage*, New Jersey: Prentice-Hall, 1995.

[6] W. H. Press, W. T. Vetterling, S. A. Teukolsky, and B. P. Flannery, *Numerical Recipes in C*, New York: Cambridge University Press, 1992.

[7] J. K. Townsend and K. S. Shanmugan, "On Improving the Computational Efficiency of Digital Lightwave Link Simulation," *IEEE Transactions on Communications*, vol. 38, no. 11, pp. 2040–2048, November 1990.